Microbial activity in surficial sediments overlying acoustic wipeout zones at a Gulf of Mexico cold seep

Laura L. Lapham

Department of Marine Sciences, University of North Carolina at Chapel Hill, Chapel Hill, North Carolina 27599, USA

Now at Department of Oceanography, Florida State University, Tallahassee, Florida 32302, USA (lapham@ocean.fsu.edu)

Jeffrey P. Chanton

Department of Oceanography, Florida State University, Tallahassee, Florida 32302, USA

Christopher S. Martens

Department of Marine Sciences, University of North Carolina at Chapel Hill, Chapel Hill, North Carolina 27599, USA

Ken Sleeper and J. Robert Woolsey

Center for Marine Resources and Environmental Technology, University of Mississippi, University, Mississippi 38677, USA

[1] Down core concentration gradients of dissolved methane and sulfate; isotope gradients of methane, dissolved inorganic carbon, and authigenic carbonate; and organic matter elemental ratios are incorporated into a vent evolution model to describe spatial and temporal variability of sedimentary microbial activity overlying acoustic wipeout zones at Mississippi Canyon (MC) 118, Gulf of Mexico. We tested the hypothesis that these zones indicate areas where sediments are exposed to elevated fluid flux and therefore should contain saturated methane concentrations and enhanced microbial activity from sulfate reduction (SR), anaerobic oxidation of methane (AOM), and methanogenesis (MP). Thirty surficial cores (between 22 and 460 cm deep) were collected from sediments overlying and outside the wipeout zones and analyzed for pore water and solid phase constituents. Outside the wipeout zones, sulfate and methane concentrations were similar to overlying-water values and did not vary with depth; indicating low microbial activity. Above the wipeouts, nine cores showed moderate activity with gently sloping sulfate and methane concentration gradients, methane concentrations $<20 \ \mu M$, and isotope depth gradients indicative of organic matter oxidation. In stark contrast to this moderate activity, four cores showed high microbial activity where sulfate concentrations were depleted by ~ 50 cm below seafloor, maximum methane concentrations in the decompressed cores were above 4 mM, and down core profiles of $\delta^{13}C\text{-}CH_4$ and $\delta^{13}C$-dissolved inorganic carbon (DIC) indicated distinct depth zones of SR, AOM, and MP. Bulk organic matter analysis suggested that the high activity was supported by an organic source that was enriched in carbon (C:N ~ 15) and depleted in $\delta^{15}N$ and $\delta^{13}C$ compared to other activity groups, possibly due to the influx of petroleum or chemosynthetically fixed carbon. Within high activity cores, the $\delta^{13}C$-DIC values were similar to the $\delta^{13}C\text{-}CaCO_3$ values, a result expected for authigenic carbonate recently precipitated. However, these values were dissimilar in moderate activity cores, suggesting that microbial activity was higher in the past. This study provides evidence that the fluid flux at MC 118 varies over time and that the microbial activity responds to such variability. It also suggests that sediments overlying wipeout zones are not always saturated with respect to methane, which has implications for the formation and detection of gas hydrate.

1. Introduction

[2] The Gulf of Mexico hosts many cold seeps along the Texas-Louisiana continental shelf and slope [*MacDonald et al.*, 1996; *Sassen et al.*, 2004]. These seeps are fed by upwardly advecting hydrocarbon-rich fluids migrating along faults and fissures created by sedimentary, salt-driven tectonics [*Kennicutt et al.*, 1988; *Roberts et al.*, 1999b; *Salvador*, 1987]. As these fluids reach the sediment-water interface, entrained gases may become crystallized into gas hydrate under appropriate pressure and temperature conditions and form the largest methane reservoir [*Kvenvolden and Lorenson*, 2001; *Milkov*, 2004]. However, if fluid migration is fast enough, these gases may escape the sediments through bubble plumes or mud volcanoes [*Dimitrov*, 2003; *Milkov et al.*, 2003], providing a source of methane and hydrocarbons to the overlying water column. Seeping organic-rich fluids also support a diverse community of chemosynthetic organisms [*Brooks et al.*, 1987; *Childress et al.*, 1986; *Fisher et al.*, 1997, 2000] and sedimentary microbial populations [*Lanoil et al.*, 2001; *Lloyd et al.*, 2006; *Martinez et al.*, 2006; *Mills et al.*, 2003], producing unique seep deposits such as carbonate reefs and chimneys [*Roberts and Aharon*, 1994; *Sassen et al.*, 2004]. Since these communities oxidize methane entrained in the fluids, they play an important role in the ultimate fate of the methane and the spatial extent of their activity needs to be better understood.

[3] Microbial activity at seep sites is dominated by sulfate reduction (SR), anaerobic methane oxidation (AOM), and methane production (MP) [*Aharon and Fu*, 2000; *Arvidson et al.*, 2004; *de Beer et al.*, 2006; *Joye et al.*, 2004; *Orcutt et al.*, 2005]. Sulfate reduction anaerobically reduces seawater sulfate to sulfide through the oxidation of organic carbon. The sources of organic carbon at seep sites include photosynthetically fixed organic matter from the upper water column, biomass from chemosynthetic communities, and petroleum and methane entrained within upward seeping fluids. While the oxidation of all these sources leads to the higher rates of sulfate reduction measured at seep sites, much attention has focused on determining spatial variability in rates of AOM because microbial oxidation apparently consumes 90–95% of the methane before it leaves the sediments [*Reeburgh*, 1996]. Recent work has identified the microbial consortium carrying out this process [*Boetius et al.*, 2000; *Hoehler et al.*, 1994]. Regardless of the source of carbon, microbial activity produces dissolved inorganic carbon (DIC) leading to authigenic carbonate mineral precipitation [*Aharon et al.*, 1997; *Ferrell and Aharon*, 1994], thus sequestering large amounts of methane or petroleum derived carbon [*Sassen et al.*, 2004]. When dissolved sulfate is exhausted, the in situ biogenic production of methane commences [*Martens and Berner*, 1974].

[4] The relative upward fluid flux at seep sites may wax and wane over time and such temporal variability can be followed by the presence of unique seafloor features [*Hovland*, 2002; *León et al.*, 2007; *Roberts and Carney*, 1997; *Roberts*, 2001]. *Roberts and Carney* [1997] first described the relationship between seafloor features found in the Gulf of Mexico and the fluid flux via a vent evolution model. This model described high fluid flux areas as "mud prone" vents that are typically associated with mud volcanoes and devoid of biology. As the fluid flux slows, the mud prone vents calm and allow for microbial and macrofaunal activity to increase. These "transitional" vents are therefore associated with bacterial mats, chemosynthetic communities, gas hydrates, and small authigenic carbonate precipitation. The growth of bacterial mats and precipitation of car-
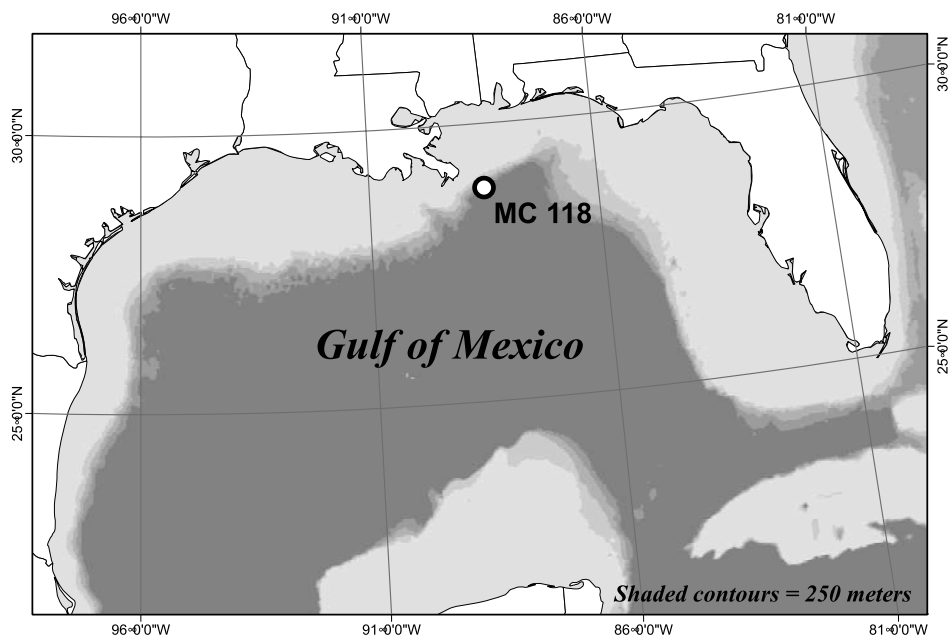
Figure 1. Map of Gulf of Mexico and close-up of Mississippi Canyon 118 (MC 118), 850 m water depth. Map courtesy of the Gulf of Mexico Hydrates Research Consortium.

bonates on the sediment surface may act to seal off the high flow path [*Hovland*, 2002]. When the fluid flux ceases, a "mineral prone" vent is left with carbonates and dead shells. This succession was also reported from video surveys in the Gulf of Cádiz [*León et al.*, 2007].

[5] Since microbial activity is an important aspect of these vent evolution models, the first objective of this study was to determine the spatial and temporal distribution of microbial activity and methane at a Gulf of Mexico seep. This information will allow us to refine the seep evolution models by including the geochemical results we obtain. The site chosen was Mississippi Canyon Lease Block 118 (MC 118), Gulf of Mexico, located offshore southern Louisiana in ~890 m of water (28°51.47, 88°29.52; Figure 1). Thorough discussions of the MC 118 complex natural system are given by *Sassen et al.* [2006] and *Lutken et al.* [2006]. Briefly, MC 118 is a fault migration-conduit overlying shallow salt that connects to deeply buried source rocks for gas and oil [*Sassen et al.*, 2006]. It is flanked on the west by the main Mississippi Canyon, formed during lower stand sea level, and a smaller, fault controlled, canyon to the east [*Woolsey et al.*, 2005]. Several submersible missions to the seafloor have identified large gas hydrate outcrops (Figure 2), authigenic carbonate mounds, several bubble and oil vents, and chemosynthetic communities including ice worms (*Sassen*

and Roberts's [2004] JRW cruise observations). The presence of these features provides evidence of variable fluid flux rates over time [i.e., *Roberts*, 2001]. Hydrate-bound gas and bubble vent gas at MC 118 have δ^{13}C-CH$_4$ values of around −47‰ and contains a mixture of methane, ethane, and propane, signifying primarily a thermogenic origin [*Sassen et al.*, 2006].

[6] Chosen as the site for a long-term gas hydrate monitoring station [*Woolsey et al.*, 2005], MC 118 has been extensively scanned using an autonomous underwater vehicle equipped with dual frequency (120 and 240 kHz) side-scan sonar and a 2–10 kHz chirp sonar subbottom profiler [*Sleeper et al.*, 2006]. From these scans, areas of high backscatter (Figure 3a) and acoustic wipeout zones (Figure 3b) have been identified within an area of 800 m by 1050 m. Although these acoustic anomalies could be due to a number of causes including authigenic carbonates, outcropping or buried hydrate, and sediments homogenized by the activity of mud volcanoes that are typically found in hydrocarbon seeps, the more accepted cause is gas bubbles [*Bouma et al.*, 1990; *Gorgas et al.*, 2003; *Kim et al.*, 2004; *Roberts et al.*, 1999a; *Sager et al.*, 1999]. For this study, we hypothesized that the wipeout zones indicate areas of higher fluid flux and therefore, contain saturated concentrations of methane and higher microbial activity from SR, AOM, and MP. We tested this hypothesis by collecting

Figure 2. Composite photo of large hydrate outcrop, located near core 25 on Figure 3a, with sediment drape and ice worms (original photos courtesy of Johnson-SeaLink submersible and mosaic courtesy of P. Mitchell, University of Mississippi).

thirty shipboard cores overlying and outside the wipeout zones and measuring down core profiles of methane and sulfate concentrations, methane and dissolved inorganic carbon isotope ratios, and organic matter chemical composition. This also gave us an opportunity to ground truth the surface expression of the seismic anomalies. Apparent microbial activity was assessed by evaluating trends in concentration and isotope depth gradients suggestive of microbial activity, as in the work by *Alperin et al.* [1988] and *Whiticar* [1999].

2. Methods

2.1. Core Collection

[7] Thirty cores were collected; one push core and 29 gravity cores (Figure 3a). The push core (PC4414) was collected in August 2002 with the Johnson Sea-Link manned submersible deployed from the Research Vessel (R/V) *Seward Johnson*. The push core was collected ~2 m from hydrate outcrop using a 30 cm long, 5 cm diameter Lexan core barrel. In May and October 2005, 29 gravity core attempts were made on two cruises off the R/V *Pelican* (operated by Louisiana Universities Marine Consortium). Core positions were targeted using previously collected chirp sonar subbottom profile data (Figure 3b) [*Sleeper et al.*, 2006]. For the May cruise, core numbers 1–10 were collected and locations determined by the ship's GPS. For the October cruise, cores 21–39 were collected and locations determined by the presence of an ultra

short baseline transponder (USBL; LinkQuest Inc., California) connected to the core barrel wire. Core depths ranged between 22 and 460 cm below seafloor (bsf) (see auxiliary material[1] Table S1). The USBL was calibrated to have an accuracy of about 8 m (P. Higley, personal communication, 2007). It should be noted that the core numbers given in Figure 3a correspond to a radius of about 25 m and therefore, accurately represent the core locations.

2.2. Core Sampling

[8] The submersible push core was sectioned every 2–3 cm and pore waters were expressed by pressure filtration [*Reeburgh*, 1967]. Two milliliters of pore water was stored at 4°C in 2 mL o-ring sealed plastic microcentrifuge tubes and frozen for later analysis of dissolved sulfate and chloride by ion chromatography [*Crill and Martens*, 1983]. The remaining pore water volume was placed in evacuated glass vials for determination of dissolved inorganic carbon (DIC) stable carbon isotope ratios. The sediment patties from the pressure filtration were frozen in plastic bags for determination of total organic carbon (TOC) and total organic nitrogen (TON) concentrations and stable carbon isotope ratios.

[9] The gravity cores were sliced lengthwise; one half was used for physical descriptions (data not

_____
[1]Auxiliary materials are available in the HTML. doi:10.1029/2008GC001944.
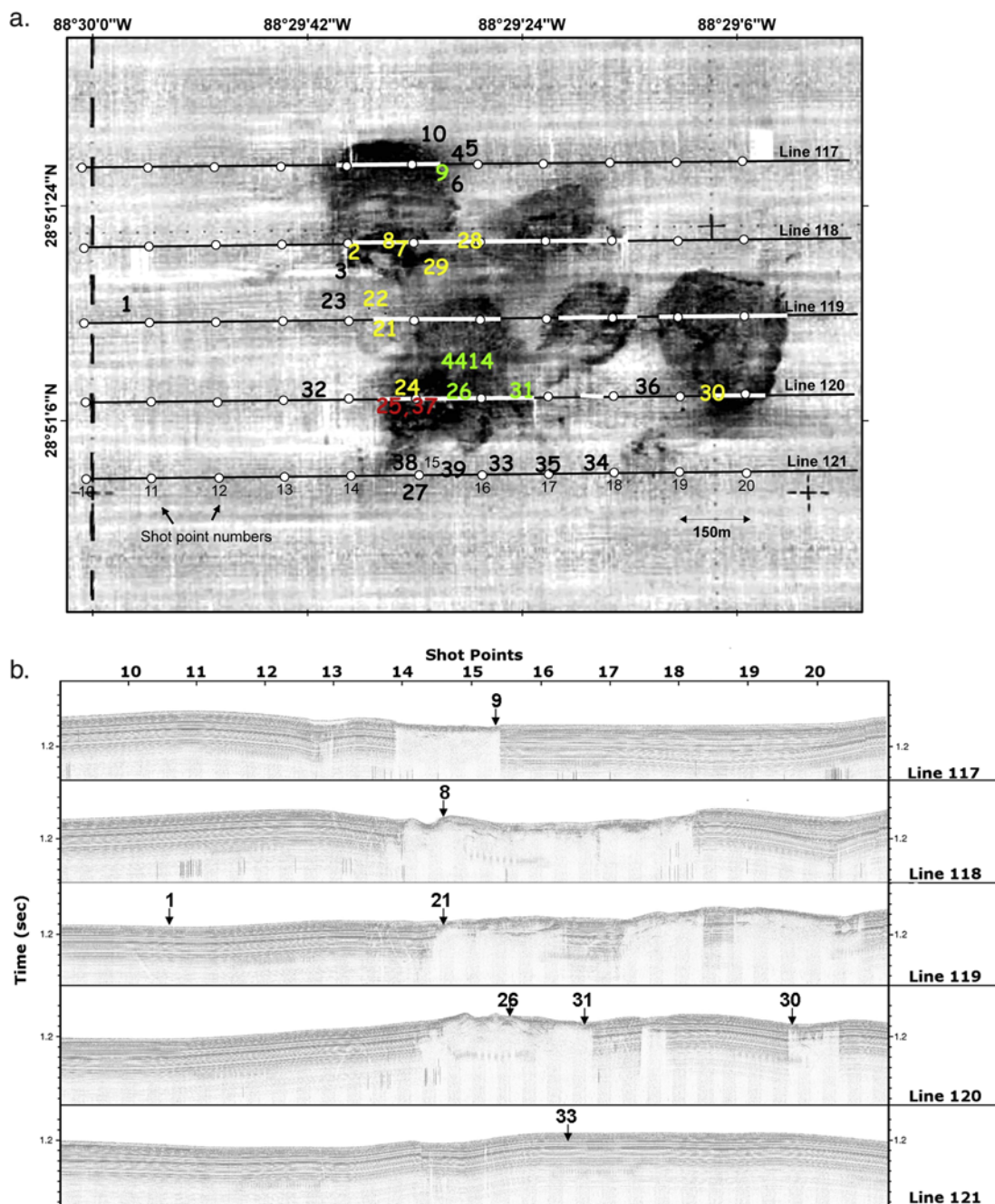
Figure 3. Geophysical maps with cores. (a) Side-scan sonar plan view map looking down at MC 118. Dark background splotches are areas of high backscatter. Ship track lines are numbered 117–121. Along these tracks, white circles and white segments relate to shot points and wipeout zones, respectively, from the chirp profiles. Colored numbers overlay where all cores were collected. Black, yellow, and green core numbers exhibit microbial activity that is low, moderate, and high, respectively. Red numbers indicate cores that returned no sediment and only carbonate. Cores 24 and 29 also contained carbonate pieces. (b) Chirp subbottom profiles for ship track lines with shot points for reference. Eight representative cores are shown. Depth of core penetration is given in text.

presented here) and the other half was sampled for geochemistry. Every 50 cm along the core, sediment plugs (6–9 mL) were collected using a 3 mL cutoff plastic syringe and placed into 30 mL glass serum vials, capped, and frozen for future analysis of methane concentrations, stable carbon isotope ratios, and porosity. The remaining sediment from each interval was collected into two 15 mL centri-

fuge tubes that were centrifuged at 3000xg for 5 min. The supernatant was transferred to 2 mL o-ring sealed plastic microcentrifuge tubes for sulfate and chloride concentration analysis while the remaining fluids were injected into evacuated 7 mL glass serum vials and frozen for determination of DIC stable carbon isotope ratios. Pore fluids were not protected against sulfide oxidation, where sulfide chemically reacts with oxygen to form sulfate. This could be a potential problem where sulfate is low and sulfide is high; traditionally near the SMTZ. Within each core, carbonate nodules were hand-picked and stored frozen for stable carbon isotope ratio analysis.

2.3. Analytical Methods

[10] Dissolved methane concentrations were measured on a Shimadzu Mini II Gas Chromatograph (GC, Kyoto, Japan) equipped with a flame ionization detector. Sample vials were injected with 10 mL methane-free deionized water, agitated to extract dissolved methane, and subsampled with two 5 mL headspace aliquots that were injected into the GC through a 1 mL external sample loop and onto a Poropak Q column at 60°C for gas separation. Resultant sample peak areas were compared to standard peak areas (Scotty, 101.6 ppm CH_4) to obtain ppm values of CH_4. Dissolved methane concentrations were then calculated via the following equation:

$$CH_4(\mu M) = \frac{CH_4(ppm)}{RT} \frac{(\text{vial volume} - \text{sed volume})(mL)}{\text{pore fluid volume}(mL)} \cdot \frac{1}{0.95} \tag{1}$$

where R is the gas constant (0.08205 L × atm/mol × K), T is temperature in K, "vial volume" is the volume of the serum vial (mL) prior to filling with sample, "sed volume" is the volume (mL) of sediment subcore placed in vial, "pore fluid volume" was measured by weight difference between wet and dry sediments corrected for sediment density for each sample, and 1/0.95 is the known efficiency of the extraction method.

[11] Sulfate and chloride concentrations were measured by diluting 100 μL of the pore water sample with 10 mL carbonate buffer eluent and injecting into a Dionex Ion Chromatograph (Sunnyvale, California) as described by *Martens et al.* [1999]. For sulfate, chloride and methane concentrations, the precision for replicate measurements of single samples was ±3%.

[12] Stable carbon isotope ratios of methane, DIC, and carbonate nodules were obtained by directly injecting microvolumes of headspace aliquots into a continuous flow Hewlett-Packard 5890 GC equipped with a 6 m Poroplot Q column at 35°C and a Finnigan Mat Delta S (Bremen, Germany). Isotope ratios were reported using the standard "del" notation, $\delta^{13}C$ (‰)= $(R_{(sample)}/R_{(PDB\ standard)} - 1)*1000$, where R is the ratio of the heavy to light isotope (^{13}C:^{12}C). Methane headspace aliquots were obtained from vials previously measured for concentrations. DIC headspace aliquots were prepared by adding 1 mL of 70% H_3PO_4 to release DIC from sample volume. Carbonate nodule headspace aliquots were prepared by rinsing the solids with tap water, drying at 60°C for 12 h, grinding, and enclosing ∼0.5 g into a 20 mL glass serum vial. The vial was then flushed with nitrogen for 5 min and ∼1 mL of 85% phosphoric acid was added to fully convert the sample to CO_2 gas for several hours while shaking. Five microliters of the evolved CO_2/N_2 gas mixture was then directly injected into the mass spectrometer for isotopic analysis. Samples were run in duplicate and analytical error was <0.6‰.

[13] The percent TOC, stable carbon isotopic composition and C/N ratios were measured on ∼30 mg of freeze-dried sediment pellets that were vapor acidified with 12 M HCl for 12 h to remove inorganic carbon prior to flash combustion to CO_2 and N_2 on a Carlo-Erba 1500 Elemental Analyzer (CE Elantech, Inc., Milan, Italy). The effluent gas stream was introduced to a Finnigan Mat 252 IRMS (Bremen, Germany) via a modified Finnigan ConFlo interface [*Brenna et al.*, 1997].

3. Results

[14] Of the 30 cores, 15 were collected outside the wipeout zones and 15 within. All but two core attempts returned sediment. Core numbers 25 and 37 had bent core catchers and returned only carbonate pieces, indicative of hitting carbonate hard grounds. Neither core was analyzed further due to lack of material. For the remaining 28 cores, sulfate and dissolved methane concentrations and methane, dissolved inorganic carbon (DIC), and carbonate stable carbon isotope ratio profiles were measured.

[15] The depths of the wipeout zones were estimated by using the two-way travel time and assuming the speed of sound of 1500 cm s^{-1}. This estimation resulted in determining different depths of the wipeout zones for each acoustic line found in Figure 3. For acoustic line 117, the wipeout zone
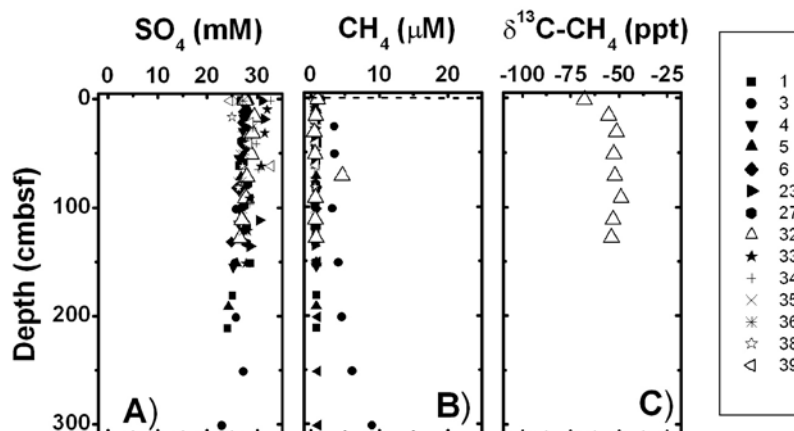
Figure 4. Low microbial activity cores collected outside wipeout zones. Depth-dependent profiles are shown of (a) sulfate concentrations, (b) methane concentrations, and (c) δ^{13}C-CH$_4$ values. Thirteen cores with nearly identical profiles are shown as black squares. Since methane concentrations were so low, only core 32 (open triangles) was analyzed for methane stable carbon isotope values. In the methane profiles, the dashed line represents the methane diffusion line based on the depth of the wipeout zone for each acoustic line and assuming saturated methane, 66,000 μM, at this depth.

was at 370 cmbsf (centimeters below surface). For line 118, it was at 1100 cmbsf. For line 119, it was found at 900 cmbsf. And, for line 120, it was found at 850 cmbsf.

[16] To organize the data, a statistical k means clustering method (statistical program JMP 6.0) was used to group the cores based on apparent microbial activity and geophysical setting. Since rates of microbial activity were not directly measured, apparent activity was characterized by the rate of sulfate depletion and maximum methane concentration. The geophysical setting was either outside or overlying a wipeout zone. Using these three criteria, three groups were assigned relative labels of low, moderate, and high microbial activity. Two caveats need to be pointed out with this cluster analysis. First, core 24 was only 13 cm long, therefore, it was too short to fully ascertain its microbial activity potential. However, the cluster analysis placed it in the moderate activity group, even though it is clearly on its way to being high activity. And second, cores 10 and 27 clustered into a fourth group, solely because there was no decrease in the sulfate concentration. For the purposes of this paper, they were placed into the low activity group. The concentration and isotope profiles are discussed in section 3.1 for each group.

3.1. Microbial Activity and Biogeochemical Gradient Groups

[17] Low microbial activity was seen in fifteen cores collected outside the wipeouts (Figure 4). In these cores, sulfate concentrations ranged between 32 mM at the sediment-water interface and 23 mM at 300 cmbsf and averaged 27 ± 3 mM over all depths (Figure 4a). The rate of sulfate depletion ranged between 0 and 0.14 mM cm^{-1}. Methane concentrations ranged between 0.2 and 10 μM for all depths, which is below the saturation concentration of 1200 μM at 1 atm, 20°C (Figure 4b). For core 32, the stable carbon isotope value of methane (δ^{13}C-CH$_4$) was -68‰ near the sediment-water interface and increased to an average value of -52 ± 2‰ below 16 cmbsf (Figure 4c).

[18] The remaining cores were collected in sediments overlying the wipeouts and fell into two microbial activity groups: moderate and high. Moderate microbial activity was inferred in nine cores where sulfate concentrations were $\sim$28 mM at the sediment-water interface and decreased to $\sim$20 mM by the bottom of the cores (Figure 5a). The rate of sulfate depletion ranged between 0.01 and 1 mM cm^{-1}. Methane concentrations were near bottom water values at the sediment-water interface and increased to a maximum of 22 μM down core (Figure 5b). For cores 21, 22, and 29, the δ^{13}C-CH$_4$ values were between -61 and -76‰ over all depths, with an average of -69 ± 4‰ (n = 17; Figure 5c). For core 30, the δ^{13}C-CH$_4$
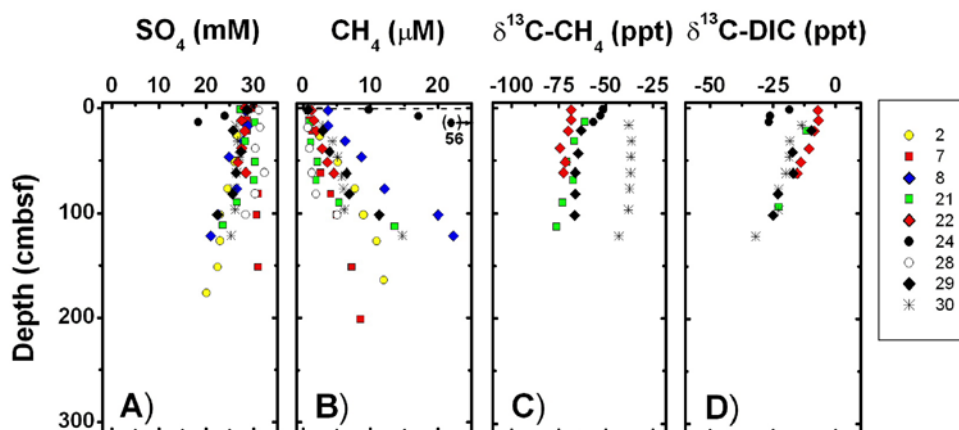
Figure 5. Moderate microbial activity cores collected within the wipeout zones. For cores, 2, 7, 8, 21, 22, 24, 28, 29, and 30, depth-dependent profiles are shown of (a) sulfate concentrations, (b) methane concentrations, (c) methane carbon isotopic composition, and (d) dissolved inorganic carbon (DIC) isotopic composition. In the methane profiles, the dashed line represents the methane diffusion line based on the depth of the wipeout zone for each acoustic line and assuming saturated methane, 66,000 μM, at this depth.

values were distinctly more enriched in ^{13}C than other cores; averaging -38 ± 4‰ (n = 7; Figure 5c). For all cores measured for δ^{13}C-DIC, the values were around -7‰ at the sediment water interface and became depleted in ^{13}C with depth to -32‰ at 100 cmbsf (Figure 5d). Core 24 exhibited steep sulfate and methane gradients even though it was a short core (only 13 cm long) and contained oil and carbonate rock (Figure 5). Sulfate concentrations were 28 mM at the sediment water interface and decreased to 18 mM at 15 cmbsf (Figure 5a). Methane concentrations were 40 μM at the sediment-water interface and increased to 231 μM

within 15 cm (Figure 5b). Although this methane gradient was high, the overall concentrations were low compared to other high microbial activity cores. At the bottom of this core, the δ^{13}C-CH$_4$ value was -56‰ (Figure 5c) and the δ^{13}C-DIC value was ~-27‰ (Figure 5d), no clear isotope trend with depth was evident because the core was too short.

[19] High microbial activity was inferred in the remaining four cores (Figure 6). In these cores, the rate of sulfate depletion ranged between 0.5 and 13 mM cm^{-1}. Since these cores exhibited very different concentration and isotope gradients, they
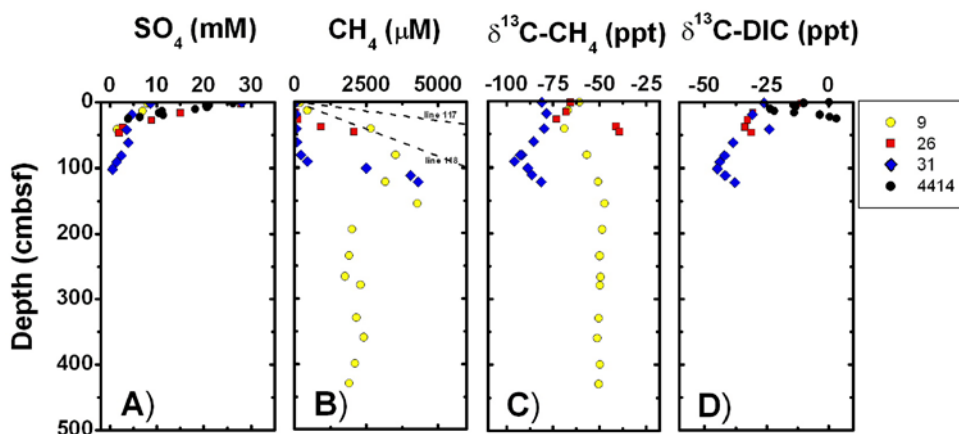

Figure 6. High microbial activity cores collected within wipeout zones. For cores 9, 26, 31, and 4414, depth-dependent profiles are shown of (a) sulfate concentrations, (b) methane concentrations, (c) methane carbon isotopic compositions, and (d) dissolved inorganic carbon (DIC) isotopic composition. In the methane profiles, the dashed lines represent the methane diffusion line based on the depth of the wipeout zone for each acoustic line (lines 117 and 118 shown) and assuming saturated methane, 66,000 μM, at this depth.

will be discussed individually. It is important to note that cores 9, 26, and 31 exhibited visible evidence of degassing and therefore, methane concentrations represent minimum values. For core 9, sulfate concentrations were around 8 mM at 1.5 cmbsf and decreased to 1 mM by 42 cmbsf (Figure 6a). This long tailing of the sulfate depletion between 1.5 and 42 cmbsf was probably due to a sulfide oxidation artifact during sample storage, therefore the sulfate was probably depleted by ~3 cmbsf. This depth is known as the sulfate-methane transition zone (SMTZ) because methane also began to increase at this depth. Methane concentrations were 190 μM near the sediment water interface and increased to 4300 μM by 120 cmbsf, exceeding methane saturation at 1 atm, 20°C (Figure 6b). Below this depth, concentrations decreased but averaged around 2000 ± 200 μM (n = 8) for the remainder of the core. The SMTZ coincided with a subsurface minimum δ^{13}C-CH$_4$ value of −70‰ (Figure 6c). Below the SMTZ, the methane became more enriched in ^{13}C to a value of −49.7 ± 1.1‰ (n = 10), indicating a narrow zone of methaneogenesis above a possible thermogenic source gas from deep below (Figure 6c). In the sediments above the SMTZ, the δ^{13}C-CH$_4$ values became enriched in ^{13}C to −60.7 ± 0.2‰, suggesting the anaerobic oxidation of methane. δ^{13}C-DIC values were not measured in this core.

[20] Sulfate concentrations in core 26 were 28 mM near the sediment-water interface and decreased to 9 mM by 47 cmbsf (Figure 6a). Below this depth, measured sulfate concentrations were ~2 mM to 50 cmbsf, probably due to the artifact of sulfide oxidation upon exposure to oxygen during sample storage. Methane concentrations were 2 μM near the sediment-water interface and increased to 2100 μM by 47 cmbsf (Figure 6b). The depth of the SMTZ was ~40 cmbsf which corresponded to a minimum δ^{13}C-CH$_4$ value of −73‰ (Figure 6c). Above and below this depth, the δ^{13}C-CH$_4$ values became enriched in ^{13}C to −65‰ near the sediment water interface and −40‰ at 50 cmbsf, respectively. The δ^{13}C-DIC also followed the same trend with a minimum value of −34‰ at the SMTZ (Figure 6d). Above this depth, the δ^{13}C-DIC values became enriched in ^{13}C to −11‰ near the sediment water interface and below this depth, the value reached −31‰ at the bottom of the core (Figure 6d).

[21] Sulfate concentrations in core 31 were 8 mM near 1.5 cmbsf, decreased to 4 mM by 20 cmbsf,

were consistently ~4 mM from 20 to 60 cmbsf, and then steadily decreased from 4 mM to 0.5 mM for the remainder of the core (Figure 6a). Methane concentrations were 11 μM near the sediment-water interface and increased to 4300 μM by 100 cmbsf (Figure 6b). The sulfate and methane concentration trends corresponded to a SMTZ depth around 90 cmbsf where the δ^{13}C-CH$_4$ values exhibited a minimum value of −95‰ (Figure 6c). Above and below this depth, the methane became enriched in ^{13}C to −80‰ (Figure 6c). The δ^{13}C-DIC values also followed the same trend with a minimum value of −50‰ at the SMTZ (Figure 6d). Above this depth, the δ^{13}C-DIC values became enriched in ^{13}C and reached −25‰ near the sediment water interface and below this depth, the values reached −37‰ (Figure 6d).

[22] Sulfate concentrations in core PC4414 were 26 mM at 1.5 cmbsf and decreased to 4 mM by 26 cmbsf (Figure 6a). Since neither methane concentrations nor isotopes were measured, the SMTZ depth was estimated to be ~10 cmbsf based on the depth of the minimum δ^{13}C-DIC value of −25‰ (Figure 6d). Above and below this depth, isotope values become enriched in ^{13}C to ~0‰ (Figure 6d). Again, these data suggest that at 26 cmbsf the 4 mM sulfate concentrations measured were probably due to the artifact of sulfide oxidation upon exposure to oxygen.

3.2. Bulk Organic Matter Chemical Composition and Stable Isotopes

[23] Within each microbial activity group, the organic matter was measured for total organic carbon (TOC) concentrations, C:N ratios, δ^{15}N total nitrogen (TN), and δ^{13}C TOC (Figure 7). These parameters were measured in a few, representative cores from each activity group due to monetary constraints. For the low activity group, cores 1 and 3 (n = 15) were measured; for the moderate activity group, cores 2, 21, 22, 29, and 30 (n = 32) were measured, and for the high activity group, cores 9, 26, 31, and 4414 (n = 44) were measured. For the low, moderate, and high activity groups, TOC concentrations were 0.47 ± 0.04%, 0.96 ± 0.36%, and 1.45 ± 1.1% (Figure 7a); C:N were 12.6 ± 2.1, 13.5 ± 0.67, and 16.0 ± 3.7 (Figure 7b); δ^{15}N TON values of 3.1 ± 0.5‰, 2.6 ± 1.1‰, and 2.3 ± 0.9‰ (Figure 7c); and δ^{13}C TOC values of 23.14 ± 1.3‰, −24.61 ± 2.7‰, and −26.17 ± 1.9‰ (Figure 7d), respectively. Using these parameters in a one-way statistical analysis test, all activity levels were significantly different
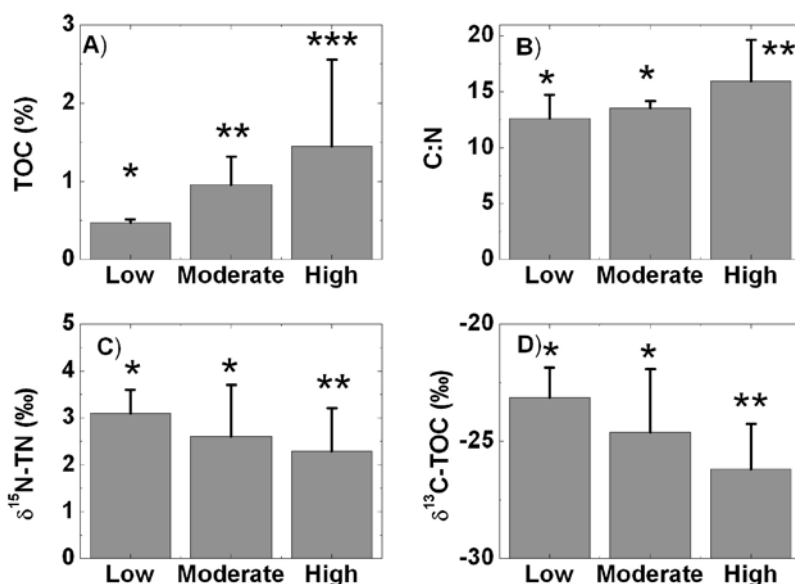
Figure 7. From representative cores within each activity group (low, moderate, and high), average values for bulk organic matter chemical composition are shown. (a) Total organic carbon (TOC) percentage, (b) carbon to nitrogen ratios, (c) δ^{15}N total nitrogen (TN), and (d) δ^{13}C TOC. Asterisk represents significantly different data sets (p value <0.05).

from each other for TOC. For C:N, δ^{15}N TN, and δ^{13}C TOC, the high activity level was significantly different from low (p value = 0.0034) and moderate (p value = 0.0102) activities.

3.3. Carbonate Nodules

[24] The stable carbon isotopic compositions of carbonate nodules ($CaCO_3$) found in cores 29, 21, 24, 26, and 31 overlying the wipeout zones were measured (Table 1). In the moderate activity group, the δ^{13}C-$CaCO_3$ values were $-28.3 \pm 0.1‰$ at 18 cmbsf in core 29 and $-30.3 \pm 0.1‰$ at 72 cmbsf in core 21. In the high activity group, the average δ^{13}C-$CaCO_3$ values were $-25.0 \pm 0.1‰$ at 13 cmbsf for core 24, $-33.6 \pm 0.3‰$ at 28 cmbsf for core 26, and $-40.8 \pm 0.1‰$ at 123 cmbsf for core 31.

4. Discussion

4.1. Spatial Distribution of Methane Concentrations Overlying Wipeout Zones

[25] We hypothesized that the wipeout zones were caused from gas bubbles trapped within the sediments and that the pore fluids above the wipeout zones would be saturated with respect to methane. At the in situ pressures, temperatures, and salinities of MC 118, saturated concentrations found in the

pore fluids surrounding bubbles would therefore be 66 mM [*Duan and Mao*, 2006]. However, because overlying water contains little to no methane, ~3 nM, the dissolved methane concentrations above the wipeout zones should fall along a diffusion line defined by the concentrations at the depth of the wipeout zone, 66 mM, and the concentrations at the sediment-water interface, 3 nM. This diffusion line assumes no anaerobic oxidation of methane which is reasonable give the lack of sulfate gradients in low and moderate activity

Table 1. Carbonate and Dissolved Inorganic Carbon Stable Carbon Isotope Ratios for the Moderate and High Microbial Activity Groups[a]

Activity Group	Core	Depth, cmbsf	δ^{13}C-$CaCO_3 \pm$ Error, ‰	δ^{13}C-DIC, ‰
Moderate	29	18	-28 ± 0.04	-8[b,c]
	21	72	-30 ± 0.08	-20[b,d]
High	24	13	-25 ± 0.10	-27 ± 0.36
	26	28	-34 ± 0.28	-33 ± 0.03
	31	123	-41 ± 0.06	-38 ± 0.28

[a] $CaCO_3$, carbonate; DIC, dissolved inorganic carbon; cmbsf, centimeters below seafloor. Error refers to standard deviation of two injections.
[b] Values were not directly measured but interpolated from down core trend line.
[c] Interpolated between measured value at 21.5 cmbsf and assumed value of 0‰ at 0 cmbsf.
[d] Interpolated between measured values at 62.5 and 93.5 cmbsf.

cores. Lines are plotted on Figures 4, 5, and 6. However, we collected sediment cores that degassed upon ascent, so the highest possible concentrations we could expect to measure is 1.2 mM, saturation at 1 atm and 25°C. Therefore, if the wipeout zones are associated with gas bubbles, we should expect measured profiles to follow the diffusion lines at concentrations below 1.2 mM, above which they would begin to fall off, due to the degassing of the core upon ascent.

[26] As expected, outside the wipeout zones, concentrations were low (<10 μM) and undersaturated with respect to methane gas. However, contrary to our hypothesis overlying the wipeouts, methane concentrations were spatially heterogeneous and below methane saturation. The majority of the cores had only moderate amounts of methane (<20 μM), although the concentrations were still greater than outside the wipeouts. Furthermore, in moderate activity cores, concentrations fell well below the diffusion line. The high activity cores exhibited the expected methane concentrations near 1200 μM, and approached the diffusion line. The anaerobic oxidation of methane may have affected these profiles as sulfate concentrations show depletion. The lack of the methane signal for the majority of the cores suggests that the wipeouts at MC 118 were not caused solely from gas bubbles. Similar results were found off the Chilean coast where an in depth integration of geophysics and geochemistry was conducted [*Coffin et al.*, 2007]. These possibilities will need to be further tested with future cores that fully penetrate the wipeout zones.

4.2. Spatial Distribution of Microbial Activity and Methane Source Overlying Wipeout Zones

[27] As hypothesized, concentration and isotope gradients showed that apparent microbial activity was higher in sediments overlying the wipeouts compared to outside them. As shown in other studies [i.e., *Aharon and Fu*, 2000; *Arvidson et al.*, 2004; *Joye et al.*, 2004], this activity was also heterogeneous, resulting in areas of both moderate and high activity. The methane source also varied spatially and was found to be both thermogenic and biogenic, following published δ^{13}C values (biogenic typically < -60‰; thermogenic >-50‰ [*Bernard et al.*, 1978], and is discussed in the following paragraphs.

[28] Except for cores 24 and 30, the moderate activity cores indicate that sulfate reduction was supported by the oxidation of organic matter rather than by methane. Several other studies have also shown that sulfate reduction is carried out by a mixture of both methane and hydrocarbon oxidation [*Joye et al.*, 2004]. Methane concentrations increased linearly with depth, suggesting methane is diffusing from below with scant consumption. The moderate activity cores had δ^{13}C-CH$_4$ values < -60‰ and did not change with depth, indicating that the source of this methane was biogenic and providing little evidence of oxidation. Little methane oxidation was also confirmed in the δ^{13}C-DIC values which were enriched in ^{13}C compared to the high activity cores. In contrast to this, the δ^{13}C-DIC values in core 24 are much more depleted in ^{13}C, suggesting methane oxidation.

[29] Although grouped within the moderate activity cores, core 30 was distinctly different than the other cores. The δ^{13}C-CH$_4$ values averaged -38 ± 4‰ which are more enriched in ^{13}C than previously reported values. They suggest either a purely thermogenic methane coming from a deep source or this methane has been highly oxidized. In order to decipher these sources, the δD-CH$_4$ values should be analyzed [*Whiticar*, 1999]. Since this core was the only core collected from the southeast mound on Figure 3a, further investigation is warranted.

[30] In contrast to the moderate activity cores, the high activity cores show distinct areas of sulfate reduction coupled to anaerobic methane oxidation, as well as methanogenesis. In depths above the SMTZ, the ^{13}C-CH$_4$ became enriched up core. This suggests anaerobic methane oxidation coupled to sulfate reduction since methane oxidation results in an enrichment of ^{13}C up core as microbes preferentially oxidize the ^{12}C contained within the methane [*Alperin et al.*, 1988; *Whiticar*, 1999]. This zone was also characterized by depletion in sulfate concentrations and concave-up profiles of methane. Below the SMTZ, δ^{13}C-CH$_4$ and δ^{13}C-DIC values also increased down core, indicating a zone of methanogenesis via carbonate reduction (as described by *Whiticar* [1999]). Core 9 penetrated below this zone of methaneogenesis and exhibited an average δ^{13}C-CH$_4$ value of -49.7 ± 1.1‰ (n = 10) over ~300 cm, indicating a thermogenic source gas from deep below. This value is similar to the δ^{13}C-CH$_4$ value of the hydrate-bound methane gas of -47‰ [*Sassen et al.*, 2006]. At MC 118, it is evident that the microbial activity and methane source are spatially heterogeneous and that there are areas of high activity or "hot spots" within the seep.

Table 2. Summary of Literature Values of Diffusive Sulfate Flux at Cold Seeps[a]

Site	Environment	SO_4^{2-} Gradient, mM cm^{-1}	Diffusive SO_4^{2-} Flux, mmol m^{-2} a^{-1}	Reference
Hydrate Ridge	*Beggiatoa* mat	8.00	7,064	*Boetius et al.* [2000]
Chile	across hydrate	0.84	742	*Coffin et al.* [2007]
Chile	across hydrate	0.03	24	*Coffin et al.* [2007]
N Cascadia Margin	near gas hydrate	0.47	277	*Pohlman* [2006]
N Cascadia Margin	near gas hydrate	0.05	31	*Pohlman* [2006]
GOM-GC 234	*Beggiatoa* mat, near hydrate	2.80	2,472	*Joye et al.* [2004]
GOM-GC 185	*Beggiatoa* mat, near hydrate	14.00	12,362	*Joye et al.* [2004]
GOM-GC 185	control site	0.00	0	*Joye et al.* [2004]
GOM-GC 233	*Beggiatoa* mat, near brine pool	1.10	971	*Orcutt et al.* [2005]
GOM-GC 232	*Beggiatoa* mat	2.14	1,892	*Orcutt et al.* [2005]
GOM-MC 118	High microbial activity	0.93	817	this study
GOM-MC 118	Moderate microbial activity	0.07	63	this study
GOM-MC 118	Low microbial activity	0.02	21	this study

[a] GOM refers to Gulf of Mexico, and GC is Green Canyon with the lease block number referenced.

[31] Since direct rates of SR and AOM were not measured in this study, the vertical sulfate diffusive fluxes were estimated to compare the activity seen at MC 118 to other cold seeps. The diffusive flux was calculated from Fick's first law:

$$J_{SO4} = -\varphi * D_s * dC/dx \qquad (2)$$

where J_{SO4} is the sulfate flux (μmol CH$_4$ cm^{-2} a^{-1}), φ is the porosity (0.8), D_s is the sedimentary methane diffusion coefficient (cm^2 s^{-1}), C is the measured sulfate concentration (mM), x is the vertical sediment depth, and dC/dx is the concentration gradient. To calculate the fluxes, D_s was 3.5×10^{-6} cm^2 s^{-1}, corrected for tortuosity and in situ pressures (87 atm at 860 m water depth), temperatures (4°C), and salinity (35 ppt) [*Millero*, 1996]. The results show that the maximum diffusive fluxes within each microbial activity grouping was 21, 63, and 816 mmol m^{-2} a^{-1} for the low, moderate, and high groups (Table 2). Values from other Gulf of Mexico hydrate sites are much higher, between 970 and 12,000 mmol m^{-2} a^{-1} [*Joye et al.*, 2004; *Orcutt et al.*, 2005]. This discrepancy could be because other studies have used submersibles to target their cores within bacterial mats, where you would expect high sulfate fluxes. From studies using gravity coring techniques, the fluxes were more similar to what was estimated at MC 118, between 25 and 740 mmol m^{-2} a^{-1} [*Coffin et al.*, 2007; *Pohlman*, 2006].

4.3. What Controls Microbial Activity in These Shallow Sediments?

[32] The spatial distribution of microbial activity at MC 118 is controlled by the heterogeneity of labile organic matter sources. At seep sites, the types of organic matter available are marine organic matter (MOM) derived from surface phytoplankton productivity, chemosynthetic community organic matter (CCOM) from local biomass including S-oxidizing bacteria and associated macrofauna, and petroleum derived from seep fluids. These types can be qualitatively assessed using chemical and stable carbon isotope ratio characteristics of the solid phase organic matter, such as δ^{13}C of total organic carbon (TOC), atomic carbon to nitrogen ratios (C:N), and δ^{15}N of total organic nitrogen (TON). The characteristic δ^{13}C values for sources are for MOM, between −18 and −22‰ [*Goni et al.*, 1997; *Peterson and Fry*, 1987], CCOM, around −27 for sulfide-oxidizing bacteria [*Larkin et al.*, 1994; *Sassen et al.*, 1993] and between −36 and −52‰ for seep macrofauna [*Brooks et al.*, 1987], and for petroleum, around −26‰ [*Kennicutt et al.*, 1988; *Wang et al.*, 2001]. The large range in CCOM isotopic values is caused by variations in the amount of methane and other carbon incorporated into seep biomass and its isotopic composition. The characteristic values for C:N ratios are not as constrained as for the δ^{13}C values. Petroleum has a C:N value >50 which is higher than the value for MOM/CCOM, typically between 6 and 10. Finally, for δ^{15}N TON values, MOM exhibits values between 5 and 15‰ [*Rau*, 1981], CCOM between −13 and 7‰ [*Brooks et al.*, 1987], and petroleum around 11‰ [*Williams et al.*, 1995].

[33] The current data set shows that the organic matter in the high activity cores is significantly enriched in TOC, has an elevated C:N ratio, and is depleted in ^{13}C and ^{15}N compared to the other cores (Figure 7). These values suggest that the sediments overlying the wipeouts are exposed to heterogeneous sources of organic matter that are

more enriched in CCOM and petroleum than MOM. Our data suggest that this heterogeneity results largely from spatial variations in the upward hydrocarbon, methane and petroleum flux, as previously hypothesized by other studies [e.g., *Joye et al.*, 2004].

4.4. Temporal Variability of Fluid Flux and Microbial Activity at MC 118

[34] Temporal variability in the fluid flux may be determined by evaluating the differences in isotopic composition between the dissolved inorganic carbon (DIC) and authigenic carbonate pools. Authigenic carbonates precipitate from pore fluids supersaturated with respect to calcium carbonate. Therefore, assuming that carbon isotope fractionation between the carbonates and bicarbonate or DIC pool was minimal [*Boehme et al.*, 1996; *Turner*, 1982], the carbonates should exhibit the stable carbon isotope values of the DIC pool at the time they were formed. As expected, the isotope values of the DIC pool and the authigenic carbonates in the high activity group of cores were similar (Table 1), suggesting that the microbial activity was high enough to sustain the recent precipitation of the carbonates. In contrast, the moderate activity cores exhibited distinctly different isotope values between the carbonates and DIC pool (Table 1). This result suggests that the carbonates are no longer precipitating at the moderate activity areas and that, at some time in the past, microbial activity had been high enough to sustain a supersaturated DIC pool and the precipitation of carbonate. This interpretation of the isotope values provides indirect evidence that supports other reports of episodic venting at seep sites [*MacDonald et al.*, 2000; *Roberts and Carney*, 1997].

4.5. Integration of Geochemical and Geophysical Data Into a Vent Evolution Model

[35] The descriptive vent evolution model first proposed by *Roberts and Carney* [1997] was modified to include geophysical and biogeochemical trends from the three microbial activity groups presented from MC 118 (Figure 8). The first phase of the integrated model begins with unaltered sediments that lack seep-related features including seismic anomalies and geochemical concentration or stable isotope gradients (Figure 8a). Such sediments were sampled at MC 118 outside the observed wipeout zones.

[36] Where the upward fluid flux is high and reaches the sediment-water interface, a high fluid flux vent containing bubble vents or mud volcanoes will result (Figure 8b). Since these fluids are typically enriched in gases, the geophysical regime is defined by acoustic anomalies that are caused by bubbles entrained within the fluids and the pore fluids should be saturated with methane. Contrary to the original descriptive model [*Roberts and Carney*, 1997], microbial activity should be the highest at these vents [*de Beer et al.*, 2006] which would be reflected in the methane and DIC isotope gradients (Figure 8b). This high flux vent was not measured at MC 118.

[37] Over time, the thermogenic fluid flux is expected to slow and a transitional, moderate flux vent form (Figure 8c). These vents contain seafloor features such as bacterial mats, other chemosynthetic communities, and gas hydrates which result in seismic anomalies. Microbial activity is still relatively high in these sediments and results in geochemical profiles as seen in the high microbial activity cores at MC 118. As carbonates precipitate from the DIC, the connection between these two carbon pools can be seen in their similar isotopic ratios.

[38] As the fluid flux ceases altogether, the transitional vent evolves into a low flux seep (Figure 8d). Because of the absence of advecting carbon substrates and reduced electron acceptors, microbial activity should slow dramatically to background values. The lack of microbial productivity then reduces the viability of the surrounding chemosynthetic communities thus limiting seafloor features to dead clam shells and authigenic carbonates. Although these seeps are no longer active, the presence of the shells and carbonates may still cause seismic anomalies, instead of gas bubbles. Other studies have also shown that wipeout zones are not always due to gas bubbles [*Coffin et al.*, 2007]. Contrary to the transitional vents, the isotopic signature of the carbonates should be indicative of past high microbial activity yet dissimilar to the current DIC pool. At MC 118, the moderate activity cores appear to represent a low fluid flux environment.

5. Conclusions

[39] In this study, we presented concentration and stable carbon isotope gradients that support both spatial and temporal variability of microbial activity within acoustic wipeout zones at a cold seep site
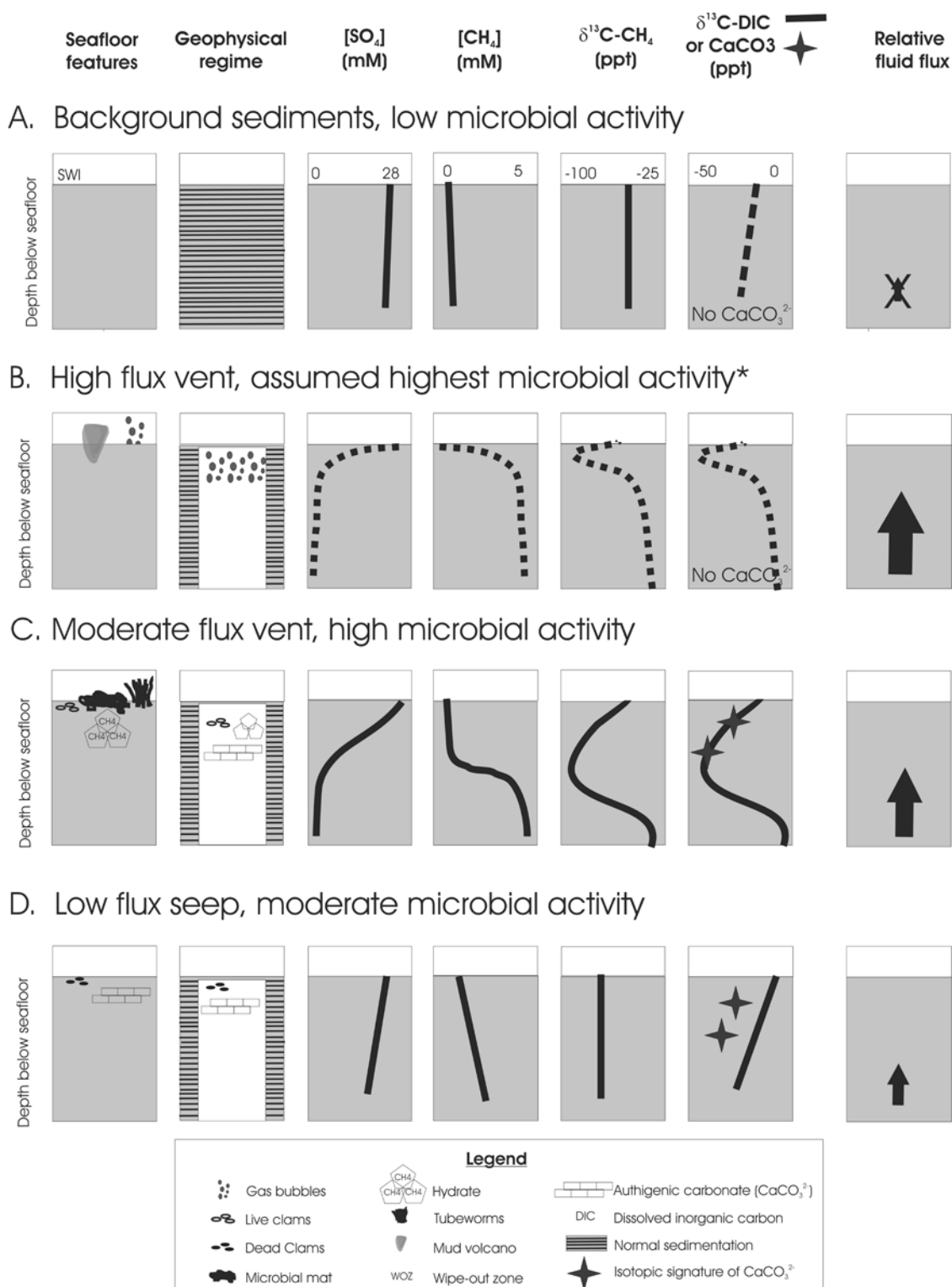
Figure 8. The integrated observational, geochemical, and geophysical seep evolution model. The asterisk in Figure 8b indicates that geochemical trends are interpreted from *de Beer et al.* [2003].

found at Mississippi Canyon 118, Gulf of Mexico. Methane concentrations and apparent microbial activity were higher in sediments overlying acoustic wipeout zones than in surrounding, unaltered sediments. However, methane concentrations were not near saturation in all cores above the wipeouts. Seismic wipeouts are frequently interpreted to result from the presence of free gas or gas hydrates. However, our results suggest that other possible causes for the wipeout zones, such as the presence of authigenic carbonates. Furthermore, the presence of carbonates may signify the remnants of a fossil seep. The extreme spatial variability in microbial activity stems from heterogeneity in the upward flux of fossil organic substrates. Finally, comparisons of the stable carbon isotopic compositions of the DIC and solid phase carbonates provide direct evidence that venting rates have waxed and waned over time due to the changes in the upward fluid flux. The proposed vent evolution model should prove useful for predicting geological, geophysical and biogeochemical characteristics of cold seeps.

Acknowledgments

References

Aharon, P., and B. Fu (2000), Microbial sulfate reduction rates and sulfur and oxygen isotope fractionations at oil and gas seeps in deepwater Gulf of Mexico, *Geochim. Cosmochim. Acta*, *64*(2), 233–246, doi:10.1016/S0016-7037(99)00292-6.

Aharon, P., H. P. Schwarcz, and H. H. Roberts (1997), Radiometric dating of submarine hydrocarbon seeps in the Gulf of Mexico, *Geol. Soc. Am. Bull.*, *109*(5), 568–579, doi:10.1130/0016-7606(1997)109<0568:RDOSHS>2.3.CO;2.

Alperin, M. J., W. S. Reeburgh, and M. J. Whiticar (1988), Carbon and hydrogen isotope fractionation resulting from anaerobic methane oxidation, *Global Biogeochem. Cycles*, *2*(3), 279–288, doi:10.1029/GB002i003p00279.

Arvidson, R. S., J. W. Morse, and S. B. Joye (2004), The sulfur biogeochemistry of chemosynthetic cold seep communities, Gulf of Mexico, USA, *Mar. Chem.*, *87*, 97–119, doi:10.1016/j.marchem.2003.11.004.

Bernard, B. B., J. M. Brooks, and W. M. Sackett (1978), Light hydrocarbons in recent Texas Continental Shelf and Slope sediments, *J. Geophys. Res.*, *83*(C8), 4053–4061, doi:10.1029/JC083iC08p04053.

Boehme, S. E., N. E. Blair, J. P. Chanton, and C. S. Martens (1996), A mass balance of ^{13}C and ^{12}C in an organic-rich methane-producing marine sediment, *Geochim. Cosmochim. Acta*, *60*(20), 3835–3848, doi:10.1016/0016-7037(96)00204-9.

Boetius, A., K. Ravenschlag, C. J. Schubert, D. Rickert, F. Widdel, A. Gieseke, R. Amann, B. B. Jorgensen, U. Witte, and O. Pfannkuche (2000), A marine microbial consortium apparently mediating anaerobic oxidation of methane, *Nature*, *407*, 623–626, doi:10.1038/35036572.

Bouma, A. H., H. H. Roberts, and J. M. Coleman (1990), Acoustical and geological characteristics of near-surface sediments, upper continental slope of northern Gulf of Mexico, *Geo Mar. Lett.*, *10*, 200–208, doi:10.1007/BF02431066.

Brenna, J. T., T. N. Corso, H. J. Tobias, and R. J. Caimi (1997), High-precision continuous-flow isotope ratio mass spectrometry, *Mass Spectrom. Rev.*, *16*, 227–258, doi:10.1002/(SICI)1098-2787(1997)16:5<227:AID-MAS1>3.0.CO;2-J.

Brooks, J. M., M. C. Kennicutt II, C. R. Fisher, S. A. Macko, K. Cole, J. J. Childress, R. R. Bidigare, and R. D. Vetter (1987), Deep sea hydrocarbon seep communities: evidence for energy and nutritional carbon sources, *Science*, *238*, 1138–1142, doi:10.1126/science.238.4830.1138.

Childress, J. J., C. R. Fisher, J. M. Brooks, M. C. Kennicutt II, R. R. Bidigare, and A. E. Anderson (1986), A methanotrophic marine molluscan (bivalvia, mytilidae) symbiosis: Mussels fueled by gas, *Science*, *233*, 1306–1308, doi:10.1126/science.233.4770.1306.

Coffin, R., J. Pohlman, J. Gardner, R. Downer, W. Wood, L. Hamdan, S. Walker, R. Plummer, J. Gettrust, and J. Diaz (2007), Methane hydrate exploration on the mid Chilean coast: A geochemical and geophysical survey, *J. Petrol. Sci. Eng.*, *56*(1–3), 32–41, doi:10.1016/j.petrol.2006.01.013.

Crill, P. M., and C. S. Martens (1983), Spatial and temporal fluctuations of methane production in anoxic coastal marine sediments, *Limnol. Oceanogr.*, *28*(6), 1117–1130.

de Beer, D., E. J. Sauter, H. Niemann, N. Kaul, J. P. Foucher, U. Witte, M. Schluter, and A. Boetius (2006), In situ fluxes and zonation of microbial activity in surface sediments of the Hakon Mosby Mud Volcano, *Limnol. Oceanogr.*, *51*(3), 1315–1331.

Dimitrov, L. I. (2003), Mud volcanoes- a significant source of atmospheric methane, *Geo Mar. Lett.*, *23*, 155–161, doi:10.1007/s00367-003-0140-3.

Duan, Z., and S. Mao (2006), A thermodynamic model for calculating methane solubility, density, and gas phase composition of methane-bearing aqueous fluids from 273 to 523 K and from 1 to 2000 bar, *Geochim. Cosmochim. Acta*, *70*, 3369–3386, doi:10.1016/j.gca.2006.03.018.

Ferrell, R. E.Jr., and P. Aharon (1994), Mineral assemblages occurring around hydrocarbon vents in the northern Gulf of Mexico, *Geo Mar. Lett.*, *14*, 74–80, doi:10.1007/BF01203717.

Fisher, C. R., I. A. Urcuyo, M. A. Simpkins, and E. Nix (1997), Life in the slow lane: Growth and longevity of cold-seep Vestimentiferans, *Mar. Ecol.*, *18*(1), 83–94.

Fisher, C. R., I. R. MacDonald, R. Sassen, C. M. Young, S. A. Macko, S. Hourdez, R. S. Carney, S. Joye, and E. McMullin (2000), Methane ice worms: Hesiocaeca methanicola colonizing fossil fuel reserves, *Naturwissenschaften*, *87*, 184–187, doi:10.1007/s001140050700.

Goni, M. A., K. C. Ruttenberg, and T. I. Eglinton (1997), Sources and contribution of terrigenous organic carbon to surface sediments in the Gulf of Mexico, *Nature*, *389*, 275–278, doi:10.1038/38477.

Gorgas, T. J., G. Y. Kim, S. C. Park, R. Wilkens, D. C. Kim, G. H. Lee, and Y. K. Seo (2003), Evidence for gassy sediments on the inner shelf of SE Korea from geoacoustic properties, *Cont. Shelf Res.*, *23*, 821–834, doi:10.1016/S0278-4343(03)00026-8.

Hoehler, T. M., M. J. Alperin, D. B. Albert, and C. S. Martens (1994), Field and laboratory studies of methane oxidation in an anoxic marine sediment: Evidence for a methanogen-sulfate reducer consortium, *Global Biogeochem. Cycles*, *8*(4), 451–463, doi:10.1029/94GB01800.

Hovland, M. (2002), On the self-sealing nature of marine seeps, *Cont. Shelf Res.*, *22*, 2387–2394, doi:10.1016/S0278-4343(02)00063-8.

Joye, S. B., A. Boetius, B. N. Orcutt, J. P. Montoya, H. N. Schulz, M. J. Erickson, and S. K. Lugo (2004), The anaerobic oxidation of methane and sulfate reduction in sediments from Gulf of Mexico cold seeps, *Chem. Geol.*, *205*, 219–238, doi:10.1016/j.chemgeo.2003.12.019.

Kennicutt, M. C., J. M. Brooks, and G. J. Denoux (1988), Leakage of deep, reservoired petroleum to the near surface on the Gulf of Mexico continental slope, *Mar. Chem.*, *24*, 39–59, doi:10.1016/0304-4203(88)90005-9.

Kim, D. C., G. H. Lee, Y. K. Seo, G. Y. Kim, S. Y. Kim, J. C. Kim, S. C. Park, and R. Wilkens (2004), Distribution and acoustic characteristics of shallow gas in the Korea Strait shelf mud off SE Korea, *Mar. Georesour. Geotechnol.*, *22*, 21–31, doi:10.1080/10641190490466928.

Kvenvolden, K. A., , and T. D. Lorenson (Eds.) (2001), *The Global Occurrence of Natural Gas Hydrates*, *Geophys. Monogr. Ser.,* vol. 124, edited by C. K. Paull and W. P. Dillon, 315 pp., AGU, Washington, D. C.

Lanoil, B. D., R. Sassen, M. T. LaDuc, S. T. Sweet, and K. H. Nealson (2001), Bacteria and Archaea physically associated with Gulf of Mexico gas hydrates, *Appl. Environ. Microbiol.*, *67*(11), 5143–5153, doi:10.1128/AEM.67.11.5143-5153.2001.

Larkin, J., P. Aharon, and M. C. Henk (1994), Beggiatoa in microbial mats at hydrocarbon vents in the Gulf of Mexico and warm mineral springs, Florida, *Geo Mar. Lett.*, *14*, 97–103, doi:10.1007/BF01203720.

León, R., L. Somoza, T. Medialdea, F. J. González, D. Díaz-del-Río, M. C. Fernández-Puga, A. Maestro, and M. P. Mata (2007), Sea-floor features related to hydrocarbon seeps in deepwater carbonate-mud mounds of the Gulf of Cádiz: From mud flows to carbonate precipitates, *Geo Mar. Lett.*, *27*, 237–247, doi:10.1007/s00367-007-0074-2.

Lloyd, K. G., L. Lapham, and A. Teske (2006), An anaerobic methane-oxidizing community of ANME-1b archaea in hypersaline Gulf of Mexico sediments, *Appl. Environ. Microbiol.*, *72*(11), 7218–7230, doi:10.1128/AEM.00886-06.

Lutken, C. B., C. A. Brunner, L. L. Lapham, J. P. Chanton, R. Rogers, R. Sassen, J. Dearman, L. Lynch, J. Kuykendall, and A. Lowrie (2006), Analyses of core samples from Mississippi Canyon 118, paper OTC 18208 presented at Offshore Technology Conference, Am. Assoc. of Pet. Geol., Houston, Tex.

MacDonald, I. R., J. F. Reilly, S. E. Best, R. Venkataramaiah, R. Sassen, J. Amos, and N. L. Guinasso, Jr. (1996), A remote-sensing inventory of active oil seeps and chemosythetic communities in the northern Gulf of Mexico, in *Hydrocarbon Migration and Its Near-Surface Expression*, edited by D. Schumacher, and M. A. Abrams, *AAPG Mem.*, 66, 27–37.

MacDonald, I. R., D. B. Buthman, W. W. Sagar, M. B. Peccini, and N. L. Guinasso, Jr. (2000), Pulsed oil discharge from a mud volcano, *Geology*, *28*(10), 907–910, doi:10.1130/0091-7613(2000)28<907:PODFAM>2.0.CO;2.

Martens, C. S., and R. A. Berner (1974), Methane production in the interstitial waters of sulfate-depleted marine sediments, *Science*, *185*(4157), 1167–1169, doi:10.1126/science.185.4157.1167.

Martens, C. S., D. B. Albert, and M. J. Alperin (1999), Stable isotope tracing of anaerobic methane oxidation in the gassy sediments of Eckernförde Bay, German Baltic Sea, *Am. J. Sci.*, *299*, 589–610, doi:10.2475/ajs.299.7-9.589.

Martinez, R. J., H. J. Mills, S. Story, and P. A. Sobecky (2006), Prokaryotic diversity and metabolically active microbial populations in sediments from an active mud volcano in the Gulf of Mexico, *Environ. Microbiol.*, *8*(10), 1783–1796, doi:10.1111/j.1462-2920.2006.01063.x.

Milkov, A. V. (2004), Global estimates of hydrate-bound gas in marine sediments: how much is really out there?, *Earth Sci. Rev.*, *66*, 183–197, doi:10.1016/j.earscirev.2003.11.002.

Milkov, A. V., R. Sassen, T. V. Apanasovich, and F. G. Dadashev (2003), Global gas flux from mud volcanoes: A significant source of fossil methane in the atmosphere and the ocean, *Geophys. Res. Lett.*, *30*(2), 1037, doi:10.1029/2002GL016358.

Millero, F. (1996), *Chemical Oceanography*, 460 pp., CRC Books, Boca Raton, Fla.

Mills, H. J., C. Hodges, K. Wilson, I. R. MacDonald, and P. A. Sobecky (2003), Microbial diversity in sediments associated with surface-breaching gas hydrate mounds in the Gulf of Mexico, *FEMS Microbiol. Ecol.*, *46*, 39–52, doi:10.1016/S0168-6496(03)00191-0.

Orcutt, B. N., A. Boetius, M. Elvert, V. A. Samarkin, and S. B. Joye (2005), Molecular biogeochemistry of sulfate reduction, methanogenesis, and the anaerobic oxidation of methane at Gulf of Mexico cold seeps, *Geochim. Cosmochim. Acta*, *69*(17), 4267–4281, doi:10.1016/j.gca.2005.04.012.

Peterson, B. J., and B. Fry (1987), Stable isotopes in ecosystem studies, *Annu. Rev. Ecol. Syst.*, *18*, 293–320, doi:10.1146/annurev.es.18.110187.001453.

Pohlman, J. W. (2006), Sediment biogeochemistry of Northern Cascadia Margin shallow gas hydrate systems, Ph.D. thesis, College of William and Mary, Gloucester Point, Va.

Rau, G. H. (1981), Low 15N/14N in hydrothermal vent animals: ecological implications, *Nature*, *289*(5797), 484–485, doi:10.1038/289484a0.

Reeburgh, W. S. (1967), An improved interstitial water sampler, *Limnol. Oceanogr.*, *12*, 163–165.

Reeburgh, W. S. (1996), *"SOFT SPOTs" in the Global Methane Budget*, 342 pp., Kluwer Acad., Andover, U. K.

Roberts, H. H. (2001), Fluid and gas expulsion on the northern Gulf of Mexico continental slope: Mud-prone to mineral-prone responses, in *Natural Gas Hydrates: Occurrence, Distribution, and Detection, Geophys. Monogr. Ser.*, vol. 124, edited by C. K. Paull and W. P. Dillon, pp. 145–161, AGU, Washington, D. C.

Roberts, H. H., and P. Aharon (1994), Hydrocarbon-derived carbonate buildups of the northern Gulf of Mexico continental slope: A review of submersible investigations, *Geo Mar. Lett.*, *14*, 135–148, doi:10.1007/BF01203725.

Roberts, H. H., and R. S. Carney (1997), Evidence of episodic fluid, gas and sediment venting on the northern Gulf of Mexico continental slope, *Econ. Geol.*, *92*, 863–879.

Roberts, H. H., B. Kohl, D. Menzies, and G. D. Humphrey (1999a), Acoustic wipe-out zones—A paradox for interpreting seafloor geologic/geotechnical characteristics (an exam-

ple from Garden Banks 161), paper OTC 10921 presented at Offshore Technology Conference, SPONSOR, Houston, Tex.

Roberts, H. H., R. A. McBride, and J. Coleman (1999b), Outer shelf and slope geology of the Gulf of Mexico: An overview, in *The Gulf of Mexico Large Marine Ecosystems: Assessments, Sustainability, and Management*, edited by H. Kumpf et al., pp. 93–112, Blackwell Sci., Boston, Mass.

Sager, W. W., C. S. Lee, I. R. MacDonald, and W. W. Schroeder (1999), High-frequency near-bottom acoustic reflection signatures of hydrocarbon seeps on the northern Gulf of Mexico continental slope, *Geo Mar. Lett.*, *18*, 267–276, doi:10.1007/s003670050079.

Salvador, A. (1987), Late Triassic-Jurassic paleogeography and origin of Gulf of Mexico Basin, *AAPG Bull.*, *71*(4), 419–451.

Sassen, R., and H. Roberts (2004), Site selection and characterization of vent gas, gas hydrate, and associated sediments, technical report, 227 pp., Dep. of Energy, Washington, D. C.

Sassen, R., H. H. Roberts, P. Aharon, J. Larkin, E. W. Chinn, and R. Carney (1993), Chemosynthetic bacterial mats at cold hydrocarbon seeps, Gulf of Mexico continental slope, *Org. Geochem.*, *20*, 77–89, doi:10.1016/0146-6380(93)90083-N.

Sassen, R., H. H. Roberts, R. Carney, A. V. Milkov, D. A. DeFreitas, B. Lanoil, and C. Zhang (2004), Free hydrocarbon gas, gas hydrate, and authigenic minerals in chemosynthetic communities of the northern Gulf of Mexico continental slope: relation to microbial processes, *Chem. Geol.*, *205*, 195–217, doi:10.1016/j.chemgeo.2003.12.032.

Sassen, R., H. H. Roberts, W. Jung, C. B. Lutken, D. A. DeFreitas, S. T. Sweet, and N. L. Guinasso Jr. (2006), The Mississippi Canyon 118 Gas Hydrate Site: A complex nat-

ural system, paper OTC 18132 presented at Offshore Technology Conference, sponsor, Houston, Tex.

Sleeper, K., A. Lowrie, A. Bosman, L. Macelloni, and C. T. Swann (2006), Bathymetric mapping and high resolution seismic profiling by AUV in MC 118 (Gulf of Mexico). paper OTC 18133 presented at Offshore Technology Conference, sponsor, Houston, Tex.

Turner, J. V. (1982), Kinetic fractionation of carbon-13 during calcium carbonate precipitation, *Geochim. Cosmochim. Acta*, *46*(7), 1183–1191, doi:10.1016/0016-7037(82)90004-7.

Wang, X.-C., R. F. Chen, J. K. Whelan, and L. Eglinton (2001), Contribution of "old" carbon from natural marine hydrocarbon seeps to sedimentary and dissolved organic carbon pools in the Gulf of Mexico, *Geophys. Res. Lett.*, *28*(17), 3313–3316, doi:10.1029/2001GL013430.

Whiticar, M. J. (1999), Carbon and hydrogen isotope systematics of bacterial formation and oxidation of methane, *Chem. Geol.*, *161*, 291–314, doi:10.1016/S0009-2541(99)00092-3.

Williams, L. B., R. E. J. Ferrell, I. Hutcheon, A. J. Bakel, M. M. Walsh, and H. R. Krouse (1995), Nitrogen isotope geochemistry of organic matter and minerals during diagenesis and hydrocarbon migration, *Geochim. Cosmochim. Acta*, *59*(4), 765–779, doi:10.1016/0016-7037(95)00005-K.

Woolsey, J. R., P. Higley, L. L. Lapham, J. P. Chanton, C. Lutken, K. Sleeper, R. Culp, S. Sharpe, and D. Ross (2005), Operations report of cruise GOM2-05-MC118 deployment of the initial components of the sea floor monitoring station–the pore-fluid array and the geophysical line array–via the sea floor probe system and collection of core samplers, Mississippi Canyon 118, report, 11 pp., Gulf of Mexico Hydrates Res. Consortium, Univ. of Miss. Cent. for Mar. Resour. and Environ. Technol., University.